# Design and operation of a DC/DC converter to integrate energy storage into a railway traction system

Maria R. Rogina[1], Julian Najera[1], Alberto Rodriguez[1], Iban Ayarzaguena[2], David Ortega[2], Andoni Pulido[2], Igor Larrazabal[2].
[1] University of Oviedo. Power Supply Systems group.
Campus de Viesques s/n, 33204 Gijón. Spain
[2] Ingeteam Power Technology S.A.
48170 Zamudio. Vizcaya. Spain.
Tel.: +34 – 985182092
E-Mail: rodriguezrmaria@uniovi.es, uo244000@uniovi.es, rodriguezalberto@uniovi.es, iban.ayarzaguena@ingeteam.com, david.ortega@ingeteam.com, andoni.pulido@ingeteam.com, igor.larrazabal@ingeteam.com.
URL: [1] www.uniovi.es [2] www.ingeteam.com

## Acknowledgements

This work has been supported by the "Ministerio de Ciencia, Innovación y Universidades" of the Spanish Government under projects RTI2018-099682-A-I00 and MCIU-19-PCI2019-103490, and by the European Union under project UE-18-POWER2POWER-826417.

## Keywords

Dual Active Bridge (DAB) DC-DC converter, Bi-directional converters, Silicon Carbide (SiC).

## Abstract

The use of Energy Storage Systems (ESSs) can improve the energy efficiency of railway systems assisting the traction system and recovering regenerative braking energy. In this paper, a medium frequency modular converter using SiC MOSFETs is analyzed to interface the ESS with a 1500 Vdc catenary and the load.
The use of SiC MOSFETs allows the increase of the switching frequency and the reduction of the size, volume and weight of the transformer. A modular topology can provide redundancy, fault tolerance and enables system scalability. The maximum power and switching frequency of one module is estimated using commercially available semiconductors.

## Introduction

Railway transportation is an energy-efficient transport mode, generating significantly less CO2 emissions than other modes. Improving energy efficiency is one of the most important aspects of the strategies that try to reduce CO2 emissions and costs and increase business benefits. Energy Storage Systems (ESSs) have been applied to assist the traction system and recover the regenerative braking energy, improving the energy efficiency of railway systems [1]. The energy-saving rate related to the use of ESSs is claimed to be up to 25% at a system level [2]. Supercapacitors and electromechanical batteries are the most common ESSs. Supercapacitors are widely utilized in urban rail transit systems due to their relatively higher power density, short discharging and charging time and long lifetime [3]. Electrochemical batteries, such as lead-acid, Ni-Cd, NiMH or Li-ion batteries, are with relatively high energy density leading to large energy-storage capability [1]. Due to this characteristic, batteries are widely used as stationary energy storage to absorb the regenerative braking energy from different trains in a specific electrified section [4], [5]. The use of hybrid ESSs and the capacity optimization of these systems have been previously analyzed [6], [7].

The introduction of ESS has the potential to increase design flexibility, system controllability, efficiency and reliability. However, different power electronics traction topologies are required to

interface the ESS with the traction system. A high-voltage and high-power bidirectional DC/DC converter is required to transform the voltage under medium frequency (MF) operation, providing galvanic isolation and reduction of weight and size due to the utilization of higher frequencies [8], [9].

In this paper, a modular, isolated and bidirectional DC/DC converter topology is proposed. To reduce the size and volume of the proposed converter, the switching frequency is slightly increased (between 5-10kHz) thanks to the selection of commercially available high voltage Silicon Carbide (SiC) MOSFETs. Considering the available semiconductors in the market, the maximum switching frequency and power of the DC/DC module is estimated limiting the maximum junction temperature of the switches. Moreover, average and switching simulation models of the proposed converter (using PSIM) are shown, compared and used to validate the operation of the system at different operation modes (charge and discharge of the battery, regenerative braking and operation without the catenary).

This paper is organized as follows: the general description of the proposed traction system for a railway application including ESS is described in Section II. Section III shows the topology of the selected converter, as well as the most appropriate type of semiconductors. Section IV analyzes the maximum switching frequency and power achievable by the converter using commercially available semiconductors. In Section V, the entire system is simulated in different modes of operation. Finally, the conclusions of the work are included in Section VI.

## General description of the traction system including energy storage systems (ESS)

There are different types and levels of voltage for the power supply system of electric railways. The most common power supply schemes are given in Table I. In general, DC systems are used in mass transit systems, being 1500 V and 3000 V common voltage levels.

**Table I: Voltage levels for electric railways according to EN 50163**

| **Electrification system** | **Voltage** | | |
|---|---|---|---|
| | Min. non-permanent | Nominal | Max. non-permanent |
| **600 $V_{dc}$** | 400 V | 600 V | 800 V |
| **750 $V_{dc}$** | 500 V | 750 V | 1000 V |
| **1500 $V_{dc}$** | 1000 V | 1500 V | 1950 V |
| **3 $kV_{dc}$** | 2 kV | 3 kV | 3.9 kV |
| **15 $kV_{ac}$, 16.7 Hz** | 11 kV | 15 kV | 18 kV |
| **25 $kV_{ac}$, 50 Hz** | 17.5 kV | 25 kV | 29 kV |

This paper aims to validate the operation of a combined power supply system composed of an ESS with a nominal voltage of 750 $V_{dc}$ and a 1500 $V_{dc}$ catenary (mainly used in medium power traction systems, in the range of units of MW). In Fig. 1, the scheme of the proposed traction power supply system is shown. This paper is focused on the validation of the different operation modes and the design specifications of the DC/DC converter.

The DC/DC converter must be able to operate mainly in these three operation modes:

1) Controlled charge of the ESS from the catenary: energy flows from HV bus to LV bus.
2) Charge of the ESS due to the regenerative braking: energy flows from HV bus to LV bus.
3) Regulation of the voltage of the HV bus: energy flows form LV bus to HV bus. This operation mode is only selected when the catenary is not available.

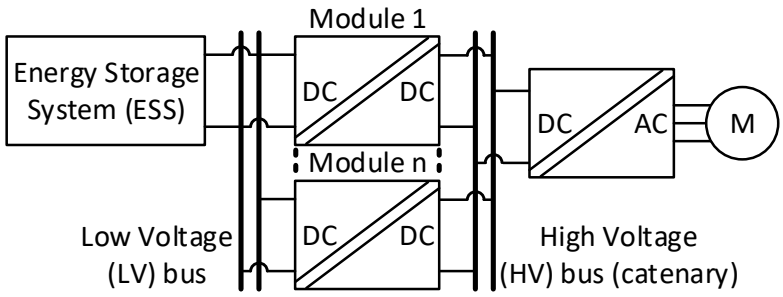


Fig. 1. Scheme of the proposed traction power supply system. The nominal output voltage of the ESS (LV bus) is 750 $V_{dc}$ while the nominal voltage of the catenary is 1500 $V_{dc}$ (HV bus).

The DC/DC converter must be bidirectional and galvanically isolated. A medium frequency transformer (5 – 10 kHz) should be used to reduce its volume and weight. The use of SiC MOSFETs is evaluated to increase the switching frequency without increasing the semiconductor junction temperature over their maximum values.

A modular DC/DC converter is designed to allow the scalability of the system. The maximum power and switching frequency of one module will be estimated using the commercially available semiconductors. The number of required modules is a function of the maximum power required by the traction power supply system. This modular solution can also provide redundancy and fault tolerance.

## Topology of the bidirectional DC-DC converter topology at medium frequency

The Dual-Active Bridge (DAB) is a widely known topology for high-power DC/DC conversions with galvanic isolation and bidirectional buck and boost operation capability [10]-[12]. Another key feature of the DAB converter is the inherent soft-switching capability with the single phase-shift (SPS) control, allowing an increase of the switching frequency. Power semiconductor devices of both bridges are switched on with zero-voltage switching (ZVS), leading to low switching losses and high efficiency. However, in light-load conditions, the benefit of the ZVS may be lost. Besides, the rms current of the transformer also increases dramatically with larger voltage variations. This can deteriorate the overall steady-state performance of the DAB converter. Alternative modulation schemes employing multiple phase-shift [13]-[19], have been proven effective to extend the soft-switching range and boost the converter efficiency and should be used under light-load conditions. The DAB can be easily parallelized because it behaves as a current source in its input and output [12], and consequently it meets all the previously described requirements.

The DAB basic topology is shown in Fig. 2. As will be shown later, the power devices of the LV bridge are 1.7 kV Silicon (Si) IGBTs while 3.3 kV SiC MOSFETs are used in the HV bridge. As it can be seen, the LV is given by the voltage of the ESS. However, the HV behavior depends on the operation mode, being emulated like a voltage source when the voltage is regulated by the catenary and like a current source when the catenary is disconnected and the HV is regulated by the DAB converter.

Fig. 3 shows some waveforms of DAB operation indicating parameters of particular interest for the calculation of the avergae and rms currents of semiconductors. Following [12] and [20] and using (1) and (2) the values of n and Lk are calculated, respectively, based on the voltages LV ($V_{LV}$) and HV ($V_{HV}$), the switching frequency ($f_{sw}$), the power ($P_{nom}$), and the maximum duty cycle($d_{max}$), selected to be able to handle the $P_{nom}$ with the nominal voltages.

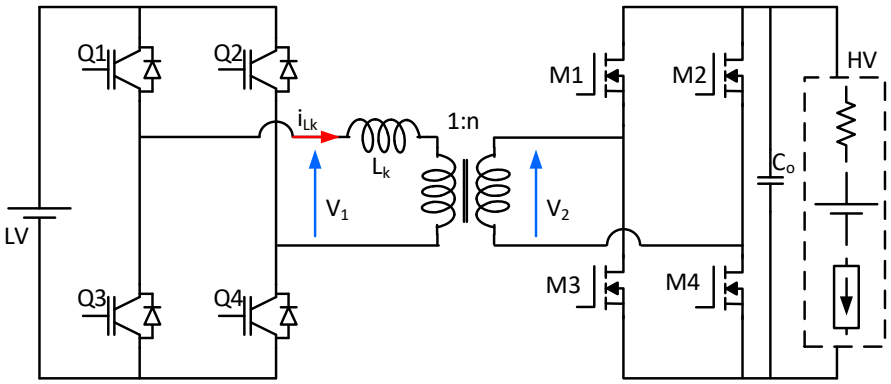


Fig. 2. Circuit diagram of the DAB converter.

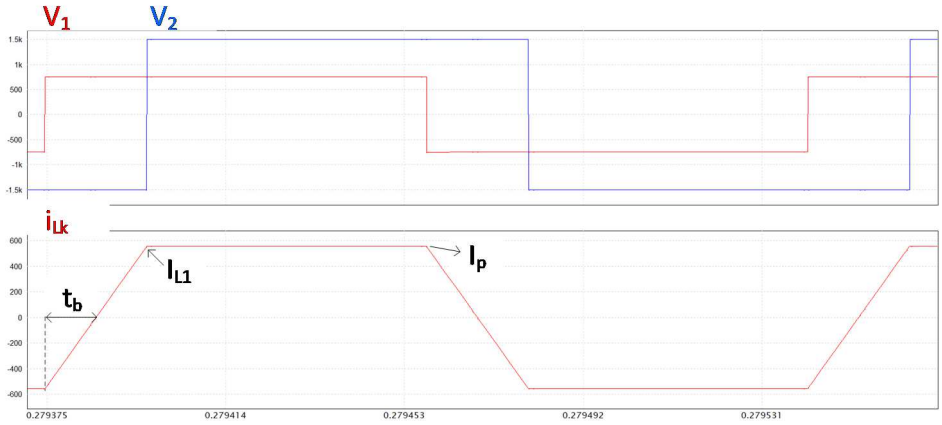


Fig. 3. DAB operating waveforms in an example case (nominal voltages, switching frequency of 6 kHz and a power of 300 kW).

$$n = \frac{V_{LV\_nom}}{V_{HV\_nom}} \tag{1}$$

$$L_k = V_{LV\_nom} \cdot V_{HV\_nom} \cdot \frac{n \cdot d_{max} \cdot (1 - d_{max})}{2 \cdot f_{sw} \cdot P_{nom}} \tag{2}$$

The leakage inductance current values at the instants of switching of both bridges can be calculated using (3) and (4). Moreover, time tb can be calculated with (5).

$$I_p = \frac{1}{4 \cdot f_{sw} \cdot L_k} \cdot \left(n \cdot V_{HV\_nom} + V_{LV\_nom} \cdot (2 \cdot d - 1)\right) \tag{3}$$

$$I_{L1} = \frac{1}{4 \cdot f_{sw} \cdot L_k} \cdot \left(n \cdot V_{HV\_nom} \cdot (2 \cdot d - 1) + V_{LV\_nom}\right) \tag{4}$$

$$t_B = \frac{n \cdot V_{HV\_nom} \cdot (2 \cdot d - 1) + V_{LV\_nom}}{4 \cdot f_{sw} \cdot \left(n \cdot V_{HV\_nom} + V_{LV\_nom}\right)} \tag{5}$$

With these values, the rms value of the leakage inductance current is obtained using (6). With this value, the rms values of the currents through the switches of both bridges are estimated using (7) and (8).

$$I_{rms\_Lk} = \sqrt{2 \cdot f_{sw} \cdot \left(\frac{I_p^2}{3} \cdot \left(\frac{d}{2 \cdot f_{sw}} - t_b\right) + \left(\frac{1}{2 \cdot f_{sw}} - \frac{d}{2 \cdot f_{sw}}\right) \cdot \left(I_p^2 + \frac{(I_p - I_{L1})^2}{3} - I_p \cdot (I_p - I_{L1})\right) + \frac{I_{L1}^2 \cdot t_B}{3}\right)} \tag{6}$$

$$I_{rms\_LV} = \frac{I_{rms\_Lk}}{\sqrt{2}} \tag{7}$$

$$I_{rms\_HV} = \frac{n \cdot I_{rms\_Lk}}{\sqrt{2}} \quad (8)$$

## Estimation of the maximum power and switching frequency of the DAB DC/DC module

Medium power traction systems usually manage power in the range of MWs. For this reason, a modular configuration looks like a promising adaptable solution. In this sense, the maximum power attainable by each module ($P_{max}$) needs to be estimated trying to increase the switching frequency and power density.

Commercially available Si IGBTs and SiC MOSFETs with breakdown voltages of 1.2 kV, 1.7 kV and 3.3 kV are compared to develop the DAB module. The maximum switching frequency and power per module for a given maximum junction temperature ($T_{jmax}$) are estimated.

Switching losses ($L_{SW}$) are estimated using turn-off energy ($E_{off}$ datasheet value is linearly extrapolated to the switching voltage and current values of the DAB converter at $P_{max}$). Turn-on energy losses ($E_{on}$) are neglected due to ZVS at full power. The current at the switching instants are estimated with (3) and (4).

Conduction losses ($L_C$) are estimated using on resistance ($R_{on}$) at $T_{jmax}$ and average and RMS current values at $P_{max}$.

Equation (9) is used to roughly compare the total losses ($L_{total}$) of all the semiconductors, where $V_0$ is 0 V for SiC MOSFETs. The junction temperature ($T_j$) of the semiconductors is estimated using (10).

$$L_{total} = L_C + L_{SW} = (V_0 \cdot I_{average}(P_{max}) + R_{on}(T_{jmax}) \cdot I^2_{rms}(P_{max})) + f_{sw} \cdot E_{off}(P_{max}) \quad (9)$$

$$T_j = R_{th\_total} \cdot \frac{L_{total}}{1000} + T_a \quad (10)$$

A preliminary approach, considering a maximum power of 250kW and a switching frequency of 5 kHz, infers that 1.7 kV/1000 A Si IGBTs are preferred for the LV side (conduction losses predominate). SiC MOSFETs switching losses reduction does not compensate for their higher conduction losses ($R_{on}$ increases considerably with the temperature) and cost. For the HV side, where switching losses predominate, 3.3 kV/750 A SiC MOSFETs result in the best option to achieve the desired switching frequency.

The total thermal resistance ($R_{th\_total}$) is the sum of the thermal resistance of the semiconductor package (extracted from the datasheet) and the heatsink (15ºC/kW and 30ºC/kW for the devices of the LV and HV bridge respectively). The ambient temperature ($T_a$) is fixed at 60ºC. The $T_{jmax}$ is fixed at 135ºC for the devices of the LV (Si) and 160ºC for the devices of the HV (SiC).

The $T_j$ at $P_{max}$ of the selected semiconductor for different switching frequencies and power is shown in Fig. 4(a). In Fig. 4(b), the power of the DAB module at which the semiconductors reach their $T_{jmax}$ for different switching frequencies is shown. An increase of the switching frequency from 1-2 kHz to 5-6 kHz allows an improvement of the power density. However, in terms of the transformer manufacturing process, an important increase in power density can be obtained rising the switching frequency to 8 kHz because a different magnetic material for the core of the transformer can be used. Mainly for this manufacturing practical reason and considering the results of Fig. 4, two different solutions are considered the best options: 300 kW at 6 kHz and 250 kW at 8 kHz. Depending on the application (space, redundancy, fault tolerance, …), a more detailed analysis should be done to find the optimal solution and the required number of modules. In this work, the maximum power of the module is $P_{max}$=300 kW and its switching frequency is $f_{sw}$=6 kHz.

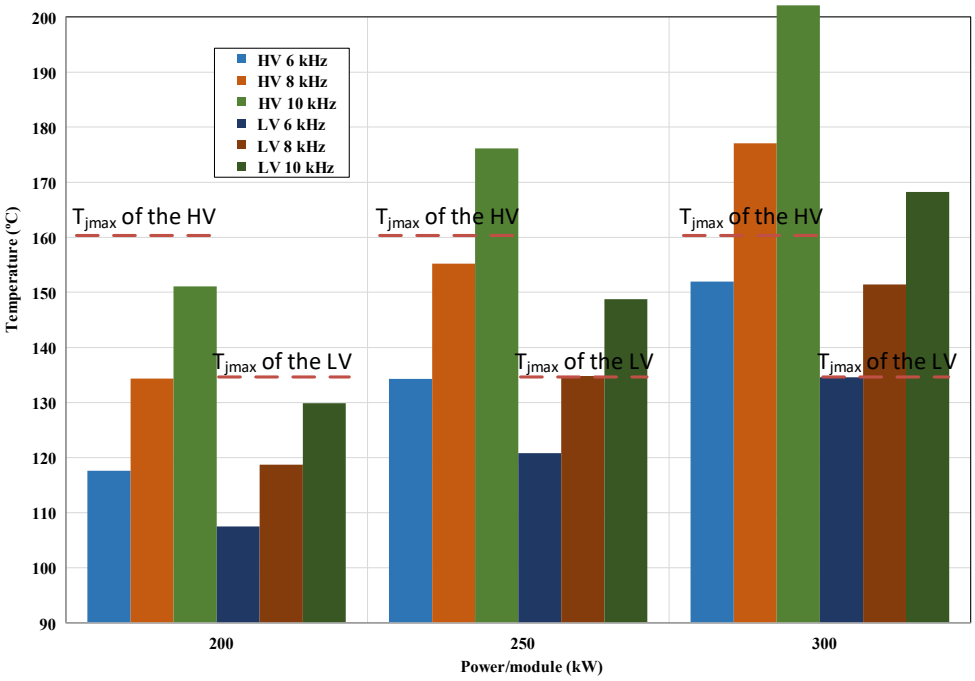


(a)

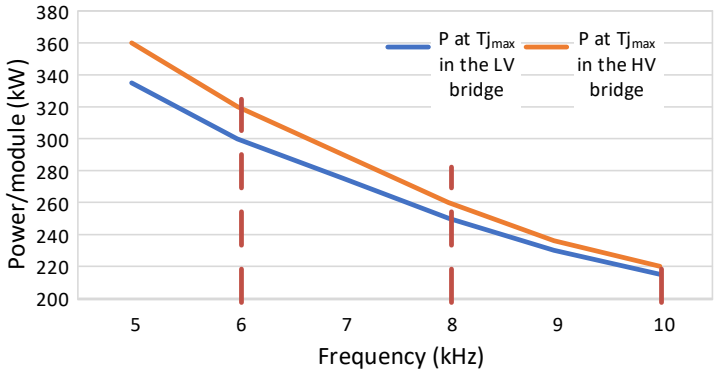


(b)

Fig. 4: (a) $T_j$ for different power and switching frequencies, for HV and LV semiconductors. (b) Power of the DAB module at which the maximum $T_j$ is reached at the selected semiconductors for LV and HV semiconductors for different switching frequencies. Examples of the estimated maximum power of the DAB module for different switching frequencies: 300 kW @ 6 kHz, 250 kW @ 8 kHz and 210 kW @ 10 kHz

## Simulation of the DAB DC/DC module at different operating modes

An average model of the DAB [12] is used to be able to simulate long simulation times in a few seconds. In Fig. 5 a comparison of the switching and average simulation model is shown. As can be seen there is good agreement in the results.

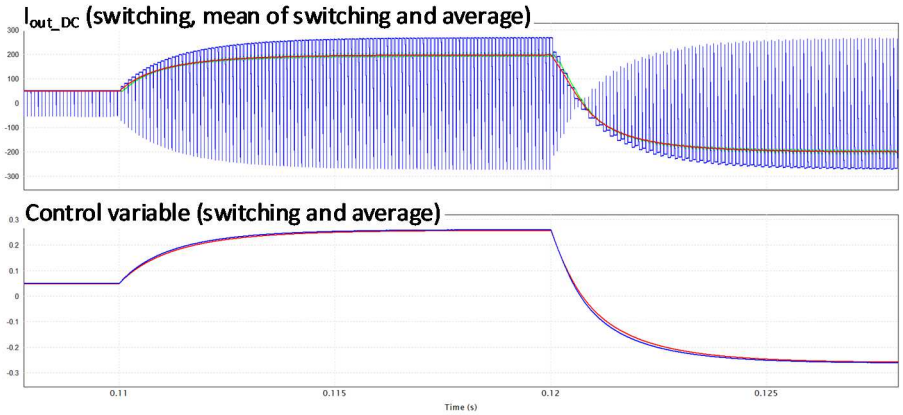


Fig. 5. Comparison of the switching (blue) and average (red) simulation models. In green, average value of the switching current. Reference current goes from 50 A (1/4 $P_{max}$) to 200 A and to -200 A.

The full system is emulated with the DAB average simulation model working in different operation modes. In Fig. 6, a diagram of the simulation is shown. The load is emulated as a current source demanding a continuous power of 1 MW. The catenary is emulated as a DC voltage source of 1500 V and a disconnection is simulated to verify that the DAB modules are able to regulate the HV bus. The ESS is emulated as a big capacitor (its capacity is adapted to simulate only a few seconds), because the technology and the capacity of the ESS (probably a hybrid one) is not fully defined yet. The control block generates the control signal used by the four modules of DAB, depending on the operation mode and the values of LV, HV and the output current of each DAB. Different high-level control strategies could be defined to optimize the energy management.

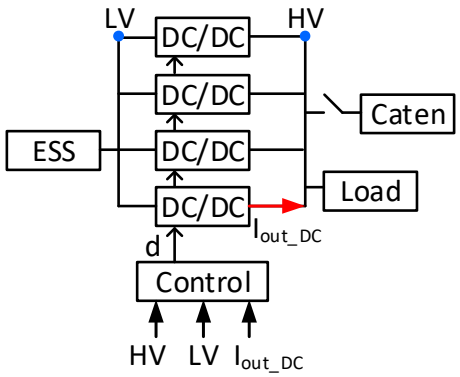


Fig. 6. Diagram of the simulated system.

As can be seen in Fig. 7, initially the ESS is charged at constant current (1/3 maximum current of the DAB module) up to its nominal voltage (750 V), when a constant voltage charge is used. The ESS is not used (the catenary supplies the load) until regenerative braking is emulated. In t= 6 s, HV is increased (1700 V) and the DAB modules absorb the maximum current to charge the battery up to its maximum voltage (780 V). If the battery is fully charged and the regenerative braking has not finished, a braking resistor should be activated to dissipate the power. At t= 10 s, the regenerative braking is finished, HV is again the nominal value of 1500 V and the battery is discharged down to its nominal value providing energy to the load. At t=18 s, the catenary is disconnected, the DAB modules supply the load and regulate HV at 1500 V. At t=22 s, the catenary is reconnected.

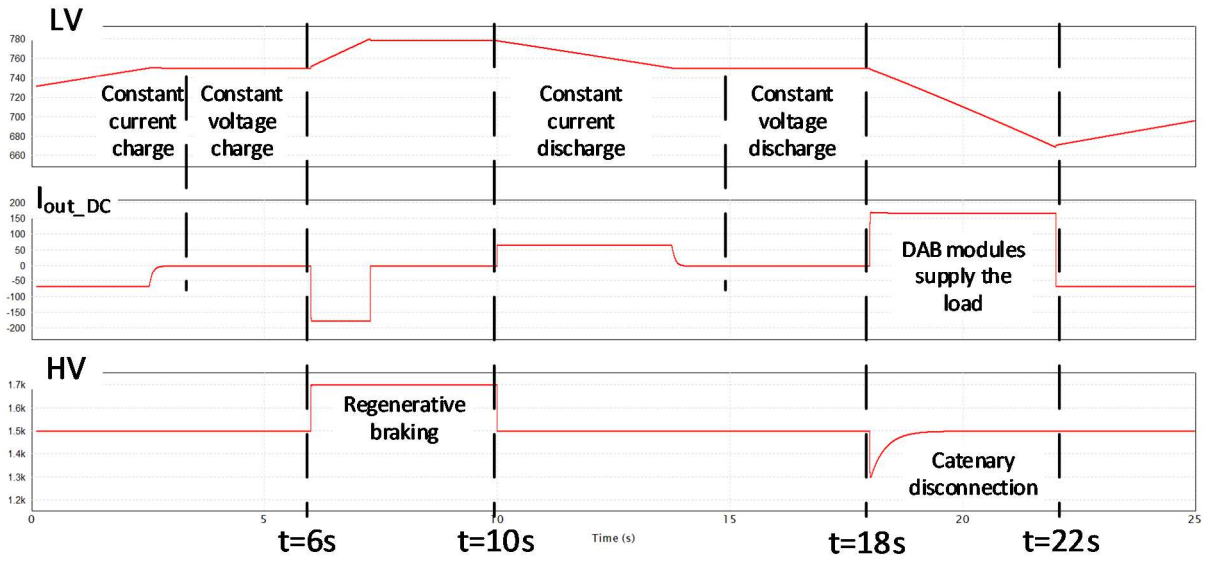

Fig. 7. Simulation results of the system in different operation modes.

## Conclusions

A bidirectional and modular solution based on an isolated DAB DC/DC converter has been proposed as an interface between the 1500 $V_{dc}$ catenary and the ESS of a railway medium power traction system.

Besides, MF operation is chosen for the topology selected in order to reduce weight and size of the system. For this aim, commercially available Si IGBTs and SiC MOSFETs are used in the simulations after being validated analytically that their maximum junction temperatures are not exceeded under a certain switching frequency operation and power demand. Using the commercially available semiconductors at this moment, a DAB converter module can be designed for a maximum power of 300 kW and a switching frequency of 6 kHz, allowing an important increase of the power density of the required medium frequency transformer. Higher switching frequency can also be obtained reducing the maximum power (200 kW at 10 kHz).

The advantages of the integration of ESS, such as the regenerative braking energy or the supply of the load without catenary, are validated using an average simulation model of the DAB and a simulation of the full system.

## References

[1] A. González-Gil, R. Palacin and P. Batty, "Sustainable urban rail systems: Strategies and technologies for optimal management of regenerative braking energy", Energy Convers. Manage., vol. 75, pp. 374-388, Nov. 2013.

[2] A. González-Gil, R. Palacin, P. Batty and J. P. Powell, "A systems approach to reduce urban rail energy consumption", Energy Convers. Manage., vol. 80, pp. 509-524, Apr. 2014.

[3] T. Ratniyomchai, P. Tricoli and S. Hillmansen, "Recent developments and applications of energy storage devices in electrified railways", IET Electr. Syst. Transp., vol. 4, no. 1, pp. 9-20, Mar. 2014.

[4] M. Ogasa, "Application of energy storage technologies for electric railway vehicles—Examples with hybrid electric railway vehicles", IEEJ Trans. Electr. Electron. Eng., vol. 5, no. 3, pp. 304-311, 2010.

[5] A. Rufer, "Energy storage for railway systems energy recovery and vehicle autonomy in Europe", Proc. Int. Power Electron. Conf. (ECCE ASIA), pp. 3124-3127, Jun. 2010.

[6] C. Wu, S. Lu, F. Xue, L. Jiang and M. Chen, "Optimal Sizing of Onboard Energy Storage Devices for Electrified Railway Systems," in IEEE Transactions on Transportation Electrification, vol. 6, no. 3, pp. 1301-1311, Sept. 2020, doi: 10.1109/TTE.2020.2996362.

[7] Tosaphol Ratniyomchai; Stuart Hillmansen; Pietro Tricoli, “Recent developments and applications of energy storage devices in electrified railways” IET Electrical Systems in Transportation. 2014. Volume: 4, Issue: 1.

[8] A. Iraklis, T. Schirmer, H. Dittus, A. Lusiewicz and J. Winter, "Overview of Three-Stage Power Converter Topologies for Medium Frequency-Based Railway Vehicle Traction Systems," in IEEE Transactions on Vehicular Technology, vol. 68, no. 4, pp. 3268-3278, April 2019, doi: 10.1109/TVT.2019.2895500.

[9] Z. Li, S. Hoshina, N. Satake and M. Nogi, "DC/DC converter development for battery energy storage supporting railway DC feeder system," 2015 9th International Conference on Power Electronics and ECCE Asia (ICPE-ECCE Asia), Seoul, 2015, pp. 1655-1660, doi: 10.1109/ICPE.2015.7167999.

[10] R. W. A. A. D. Doncker, D. M. Divan, and M. H. Kheraluwala, “A three phase soft-switched high-power-density dc/dc converter for high-power applications,” IEEE Transactions on Industry Applications, vol. 27, no. 1, pp. 63–73, Jan 1991.

[11] M. Kheraluwala, R. Gascoigne, D. Divan, and E. Baumann, “Performance characterization of a high-power dual active bridge dc-to-dc converter,” IEEE Transactions on Industry Applications, vol. 28, no. 6, pp. 1294 – 1301, Nov 1992.

[12] A. Rodríguez, A. Vázquez, D. G. Lamar, M. M. Hernando and J. Sebastián, "Different Purpose Design Strategies and Techniques to Improve the Performance of a Dual Active Bridge With Phase-Shift Control," in IEEE Transactions on Power Electronics, vol. 30, no. 2, pp. 790-804, Feb. 2015.

[13] F. Krismer and J. W. Kolar, “Efficiency-optimized high-current dual active bridge converter for automotive applications,” IEEE Transactions on Industrial Electronics, vol. 59, no. 7, pp. 2745–2760, July 2012.

[14] F. Krismer and J. W. Kolar, “Accurate small-signal model for the digital control of an automotive bidirectional dual active bridge,” IEEE Transactions on Power Electronics, vol. 24, no. 12, pp. 2756–2768, Dec 2009.

[15] F. Krismer and J. W. Kolar, "Closed Form Solution for Minimum Conduction Loss Modulation of DAB Converters," in IEEE Transactions on Power Electronics, vol. 27, no. 1, pp. 174-188, Jan. 2012.

[16] G. Oggier, G. O. García, and A. R. Oliva, “Modulation strategy to operate the dual active bridge dc-dc converter under soft switching in the whole operating range,” IEEE Transactions on Power Electronics, vol. 26, no. 4, pp. 1228–1236, April 2011.

[17] B. Zhao, Q. Song, and W. Liu, “Power characterization of isolated bidirectional dual-active-bridge dc–dc converter with dual-phase-shift control,” IEEE Transactions on Power Electronics, vol. 27, no. 9, pp. 4172–4176, Sep. 2012.

[18] N. Hou and Y. W. Li, “Overview and comparison of modulation and control strategies for a non-resonant single-phase dual-active-bridge dc–dc converter,” IEEE Transactions on Power Electronics, vol. 35, no. 3, pp. 3148–3172, 2020.

[19] A. K. Bhattacharjee and I. Batarseh, “Optimum hybrid modulation for improvement of efficiency over wide operating range for triple phase-shift dual-active-bridge converter,” IEEE Transactions on Power Electronics, vol. 35, no. 5, pp. 4804–4818, 2020.

[20] R. T. Naayagi, A. J. Forsyth and R. Shuttleworth, "High-Power Bidirectional DC–DC Converter for Aerospace Applications," in IEEE Transactions on Power Electronics, vol. 27, no. 11, pp. 4366-4379, Nov. 2012.